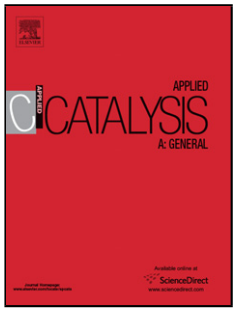

Title: Surfactant-directed mesoporous zeolites with enhanced catalytic activity in tetrahydropyranylation of alcohols: effect of framework type and morphology

Authors: Hye Sun Shin, Maksym Opanasenko, Carlos Palomino Cabello, Ryong Ryoo, Jirnullí Cnullejka

PII: S0926-860X(17)30086-8
DOI: http://dx.doi.org/doi:10.1016/j.apcata.2017.02.019
Reference: APCATA 16155

To appear in: *Applied Catalysis A: General*

Received date: 3-10-2016
Revised date: 21-2-2017
Accepted date: 24-2-2017

Please cite this article as: Hye Sun Shin, Maksym Opanasenko, Carlos Palomino Cabello, Ryong Ryoo, Jirx30c;iacute; Cx30c;ejka, Surfactant-directed mesoporous zeolites with enhanced catalytic activity in tetrahydropyranylation of alcohols: effect of framework type and morphology, Applied Catalysis A, General http://dx.doi.org/10.1016/j.apcata.2017.02.019

Surfactant-directed mesoporous zeolites with enhanced catalytic activity in tetrahydropyranylation of alcohols: effect of framework type and morphology

Hye Sun Shin[1,2], Maksym Opanasenko[3,4,*], Carlos Palomino Cabello[3], Ryong Ryoo[1,2] and Jiří Čejka[3]

[1]Center for Nanomaterials and Chemical Reactions, Institute for Basic Science(IBS), Daejeon 34141, Republic of Korea

[2]Department of Chemistry, Korea Advanced Institute of Science and Technology(KAIST), Daejeon 34141, Republic of Korea

[3]J. Heyrovský Institute of Physical Chemistry, Academy of Sciences of Czech Republic, v.v.i., Dolejškova 3, 182 23 Prague 8, Czech Republic

[4]Department of Physical and Macromolecular Chemistry, Faculty of Science, Charles University, Hlavova 8, 128 43 Prague 2, Czech Republic

*Corresponding author

Dr. Maksym Opanasenko

Department of Physical and Macromolecular Chemistry, Faculty of Science, Charles University, Hlavova 8, 128 43 Prague 2, Czech Republic; J. Heyrovský Institute of Physical Chemistry, Academy of Sciences of Czech Republic, v.v.i., Dolejškova 3, 182 23 Prague 8, Czech Republic. E-mail: maksym.opanasenko@jh-inst.cas.cz; Tel: (+420) 26605 3055

Graphical abstract

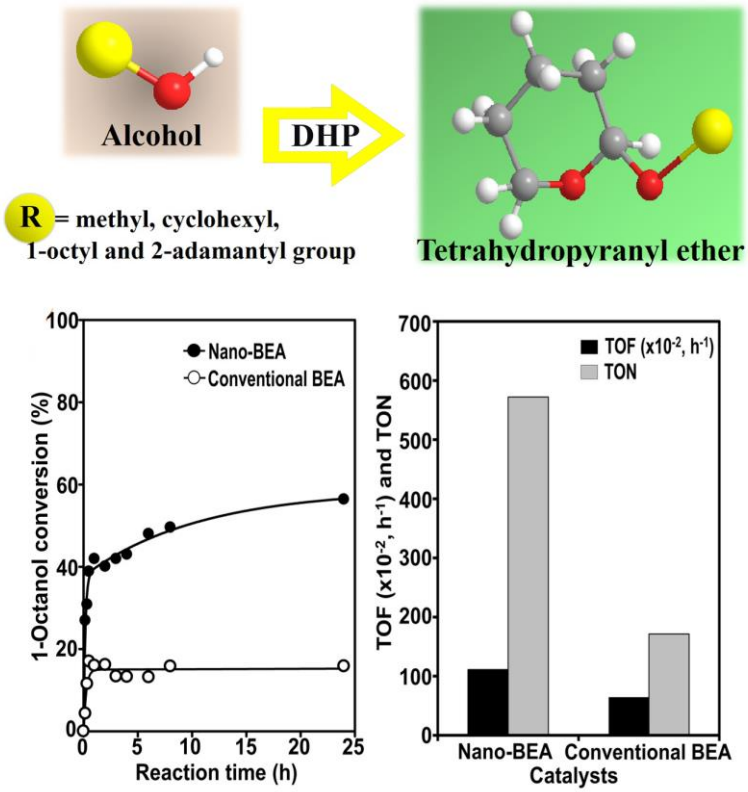

Highlights

- The influence of zeolite topology and morphology on the catalytic behaviour in tetrahydropyranylation of alcohols was investigated.
- Variables include nanosponge vs. bulk morphology, zeolite type (BEA, MTW, MFI), Si/Al and the size of reactant molecules (methanol, 1-octanol, cyclohexanol and 2-adamantanol).
- Due to the high accessibility of active sites and facile diffusion of reactant and product molecules BEA nanosponges showed enhanced catalytic performance (TON = 529 – 827) compared with conventional analogue (TON = 198 – 375).

Abstract

Nanosponge zeolite beta was hydrothermally synthesized using multi-quarternary ammonium surfactant as a meso-micro hierarchical structure directing agent. The nanosponge morphology of the beta zeolite consisted of randomly interconnected nanocrystals with thickness of 10–20 nm. The beta nanosponges with highly mesoporous structure exhibited enhanced catalytic activity in tetrahydropyranylation of alcohols (methanol, 1-octanol, cyclohexanol and 2-adamantanol) when compared with the conventional beta zeolites and nanosponge zeolites of **MTW** and **MFI** framework types. The enhanced catalytic performance (~60% conversion with 90–100% selectivity towards tetrahydropyranyl ether and over two times higher initial rate compared to other zeolites) of hierarchical beta nanosponges can be attributed to the high accessibility of acid sites and facile diffusion of reactants and products through the mesopores.

Keywords: Mesoporous beta, nanosponge zeolite, hierarchical zeolite, tetrahydropyranylation, external acidity

1. Introduction

Tetrahydropyranyl ethers have been extensively applied in organic synthesis to obtain a variety of polyfunctional compounds due to their low prices and good stability under harsh reaction conditions [1]. The tetrahydropyranyl ethers can be easily synthesized through tetrahydropyranylation reaction protecting hydroxyl groups in organic compounds with 3,4-dihydro-2H-pyran (DHP) over acid catalysts (Scheme 1).[2,3] Usually, both Brønsted acids (*e. g.* HCl [4], *p*-toluenesulfonic acid [5], *etc*) and Lewis acids (*e. g.* boron tri-fluoride etherate [6], niobium chloride [7], tantalum chloride [8], *etc*) were used as catalysts for tetrahydropyranylation of alcohols under organic solvent mediated reaction conditions. However, a mild and efficient method for tetrahydropyranylation of alcohols is required to limit the effect of moisture sensitivity of catalysts, long reaction time under reflux conditions, handling problem and environmental hazard [9,10]. In order to improve such drawbacks caused by use of the strong acids and chemical reagents, heterogeneous catalysts such as ion-exchange resins, silica-based sulfonic acid catalysts [11], natural clays [12,13], and zeolites [10,14-16] have been investigated for tetrahydropyranylation of alcohols under relatively mild reaction conditions. Particularly, zeolites have attracted much attention because of their tunable acidity, shape-selectivity, high structural stability and easy regeneration [17].

Conventional H-**FAU** **[**15] and H-beta [18] zeolites and zeolite analogues [19] (*e. g.* $AlPO_4$) were utilized in tetrahydropyranylation reaction of alcohols, phenols, naphthols including bulky substrates such as cholesterol. The H-beta zeolite exhibited high yield of target ether and good recyclability under mild reaction conditions. However, the reaction of bulky alcohols in the microporous materials proceeded slowly due to diffusion limitations requiring longer reaction times. Hence, mesoporous materials were used to resolve the diffusion restriction of bulky substrates. Nedumaran *et al*. reported that mesoporous silica synthesized by incorporation of zirconium and subsequent sulfation (*i. e.*, sulfated Zr-Si-MCM-41) exhibited an enhanced catalytic activity in

tetrahydropyranylation of phenol [20]. In addition, Corma *et al*. employed the zeolitic material (ITQ-2) with thin layered structure to increase the accessibility of active sites [21]. ITQ-2 showed higher conversions compared to H-beta zeolites in tetrahydropyranylation of bulky substrates. Most recently, Al incorporated germanosilicate **ITH** zeolites exhibited improved catalytic behavior in tetrahydropyranylation reaction, resulting from simultaneous mesoporosity and presence of strong acid centers generated by alumination treatment [22]. The additional post-treatment such as incorporation of heteroatom or delamination was necessary to introduce the strong acid sites and/or mesoporosity into the materials.

Additional strategy for the enhancement of substrate diffusion in zeolites is to decrease the diffusion path length inside the zeolite micropores by reducing the crystal or framework thickness [23-25]. The zeolites with reduced crystal thickness can be obtained through the zeolite crystallization for nanocrystal morphology or hierarchical structure possessing the secondary mesoporosity within the microporous zeolite crystals. Such zeolites with hierarchical structures have been produced in a number of synthetic routes including post-steaming [26], selective framework etching through desilication or dealumination [27,28], and addition of mesopore-generating agents (*e. g.* carbon nanoparticles [29], silylated organic polymers [30], organosilane surfactants [31-33] and multi-quarternary ammonium surfactants [34,35]) into the synthesis compositions. Particularly, the direct synthesis route for hierarchical zeolite using the organosilane or multi-ammonium surfactants as mesopore-directing agents has been well-established. The resultant zeolites exhibited remarkably enhanced catalytic activity in some catalytic reactions involving bulky molecules that fail to enter the micropores. Recently, Ryoo and coworkers reported the direct synthesis of mesoporous zeolites (*e. g.*, **MFI**, **MTW**, **MRE** and beta) with nanosponge-like morphology using multi-quarternary ammonium surfactants as meso-micro hierarchical structure directing agents (SDAs) [34-39]. The ammonium head groups and long alkyl chains of the multi-ammonium surfactants led to the formation of microporous zeolite frameworks and disordered mesostructures. Typically, nanosponge beta zeolites were synthesized using $[C_{22}H_{45}\text{-}N^{+}(CH_3)_2\text{-}C_6H_{12}\text{-}N^{+}(CH_3)_2\text{-}CH_2\text{-}(C_6H_4)\text{-}CH_2\text{-}N^{+}(CH_3)_2\text{-}C_6H_{12}\text{-}N^{+}(CH_3)_2\text{-}CH_2\text{-}(C_6H_4)\text{-}CH_2\text{-}N^{+}(CH_3)_2\text{-}C_6H_{12}\text{-}N^{+}(CH_3)_2\text{-}C_{22}H_{45}](Br^{-})_2(Cl^{-})_4$ surfactants. Moreover, Jo *et al*. proposed the synthesis method of mesoporous beta zeolite using a piperidinium-functionalized multi-ammonium surfactant as the SDA in near-neutral pH and/or high pH conditions quite recently [40]. The beta nanosponges composed of randomly assembled tiny nanocrystals possessed uniform mesopores (~4.5 nm of diameter). This nanosponge beta zeolite exhibited high catalytic performance in the Friedel-Craft alkylation of benzene [38,41], acylation of aromatic compounds [35], and Diels-Alder cycloaddition of biomass derived 2,5-dimethylfuran and ethylene [42]. The high catalytic activity of the nanosponge beta zeolite was attributed to a high concentration of strong acid sites on the external surface inducing facile diffusion of reactants and products through the mesopores. In this respect, mesoporous beta zeolite obtained via the direct synthesis can be an efficient catalyst outperforming the conventional H-beta zeolite in liquid-phase tetrahydropyranylation reaction.

The aim of this contribution was to carry out the comparative investigation of zeolite materials with different topology (beta, **MTW** and **MFI**) and morphology (nanosponge vs. bulk) as catalysts in tetrahydropyranylation of alcohols different in size (methanol,

1-octanol, cyclohexanol and 2-adamantanol). Particular attention was focused on the understanding of key reaction parameters as zeolite structure, porosity and chemical composition on the acidic properties and catalytic activity (yield, turnover frequency and turnover number) of respective materials. Since the Si/Al ratio of mesoporous beta zeolites can vary widely, materials with the Si/Al ratio of 15, 50 and 100 have been used in present study.

2. Experimental

2.1. Materials

Hexane (≥97.0%, Sigma-Aldrich), 3,4-dihydro-2H-pyran (97%, Sigma-Aldrich), methanol (Lachner), 1-octanol (Honeywell Riedel-de Haën), mesitylene (≥99.8%, Sigma-Aldrich), cyclohexanol (99%, Sigma-Aldrich) and 2-adamantanol (TCI) were used as received without further purification. Tetraethylorthosilicate (TEOS, 95%, Junsei), water glass (29 wt% SiO_2, Si/Na = 1.75, Shinheung Chemical), aluminum isopropoxide (≥98%, Sigma-Aldrich), sodium aluminate (50 - 56 wt% Al_2O_3, 40 - 45 wt% Na_2O, Sigma-Aldrich), aluminum sulfate octadecahydrate (98%, Sigma-Aldrich) and sulfuric acid (47%, Wako) were used for the synthesis of zeolites. Three kinds of zeolite SDA were prepared in the present work, according to the previous reports [37-40]. The zeolite SDAs have the molecular formulas of 4,4′-trimethylene-*bis*-[1-(CH_3)-1-{CH_2-C_6H_4-CH_2-$N^+(CH_3)_2$-C_6H_{12}-$N^+(CH_3)_2$-$C_{22}H_{45}$}piperidinium](Br^-)$_2$(Cl^-)$_4$, [$C_{22}H_{45}$-$N^+(CH_3)_2$-C_6H_{12}-$N^+(CH_3)_2$-CH_2-(C_6H_4)-CH_2-$N^+(CH_3)_2$-C_6H_{12}-$N^+(CH_3)_2$-CH_2-(C_6H_4)-CH_2-$N^+(CH_3)_2$-C_6H_{12}-$N^+(CH_3)_2$-$C_{22}H_{45}$](Br^-)$_2$(Cl^-)$_4$ and [$C_{18}H_{45}$-$N^+(CH_3)_2$-C_6H_{12}-$N^+(CH_3)_2$-C_6H_{13}](Br^-)$_2$ (See Table S1 for their molecular structure). For brevity, the three SDAs are denoted by [C_{22}-6Npipe-C_{22}](Br^-)$_2$(Cl^-)$_4$, [C_{22}-6Nph-C_{22}](Br^-)$_2$(Cl^-)$_4$ and [C_{18}-2N-C_6](Br^-)$_2$, respectively, hereafter. The purity of the zeolite SDAs was checked with ^{1}H NMR spectroscopy. Commercial zeolites (beta: CP814C* and CP811C-300, all from Zeolyst) were used for comparison in catalysis.

2.2. Preparation of zeolites

The zeolite beta nanosponges were hydrothermally synthesized using a hydroxide form of [C_{22}-6Npipe-C_{22}](Br^-)$_2$(Cl^-)$_4$ surfactant as a zeolite SDA [40]. The [C_{22}-6Npipe-C_{22}](Br^-)$_2$(Cl^-)$_4$ was ion-exchanged with OH^--exchange resin (MTO-Dowex SBR LCNG OH form, Supelco) to convert the Cl^- and Br^- ions with OH^- ions. The concentration of the hydroxide form of the surfactants in distilled water ranged from 7 to 10 wt%. For the zeolite synthesis, aluminum isopropoxide was added to an aqueous solution of [C_{22}-6Npipe-C_{22}](OH^-)$_6$ and then stirred at room temperature for 1 h. TEOS was added dropwise to the mixture solution and vigorously stirred at room temperature for 4 h. The mixture solution was placed in an oven at 333 K for 12 h. The final gel composition was 30 SiO_2: x Al_2O_3: 1.8 SDA: 5000 H_2O (x = 0.15, 0.30 and 1). After cooling down to the room temperature, the resultant mixture was transferred to a Teflon-lined autoclave and then heated at 413 K for 9 d (x = 0.15 and 0.30) or 12 d (x = 1). The solid products were collected from the aqueous solution by centrifugation, washed twice with distilled water and dried at 373 K overnight.

The **MTW** nanosponge was hydrothermally synthesized using [C_{22}-6Nph-C_{22}](Br^-)$_2$(Cl^-)$_4$ surfactant as the zeolite SDA [38]. For a typical synthesis, TEOS was dropwise

added to an aqueous solution of NaOH containing $[C_{22}\text{-}6Nph\text{-}C_{22}](Br^-)_2(Cl^-)_4$ surfactant. Sodium aluminate was dissolved in the distilled water and then the clear solution was dropwise added to the solution with continuous stirring. The resultant gel mixture was aged at 333 K for 12 h. The final synthesis gel of a composition of 100 SiO_2: 0.5 Al_2O_3: 3.3 SDA: 13 Na_2O: 4500 H_2O was transferred to a Teflon-lined stainless autoclave and then heated at 423 K for 5 d under tumbling conditions. The solid product was filtered, washed with distilled water and dried in an oven at 373 K for 12 h.

The **MFI** nanosponge was synthesized with a seed-assisted hydrothermal synthesis method using $[C_{18}\text{-}2N\text{-}C_6](Br^-)_2$ as the zeolite SDA, following the previous procedure with a slight modification [37]. The aluminum sulfate octadecahydrate was dissolved in distilled water. The solution was added to the mixture of aqueous NaOH solution, SDA and H_2SO_4 (47%). The mixture was stirred for 30 min at room temperature. Then, water glass was added dropwise with vigorous stirring. The gel mixture was stirred at 333 K for 2 h and subsequently, a calcined commercial **MFI** zeolite was added to the gel mixture as a seed, amounting to 5 wt% of total silica source. The final gel composition was 100 SiO_2: 1 Al_2O_3: 7.5 SDA: 30 Na_2O: 17 H_2SO_4: 5000 H_2O in molar ratio. The final mixture was further stirred in an oven at 333 K for 12 h and then heated at 423 K for 3 d in a Teflon-lined autoclave under agitation conditions. The solid product was filtered, washed with distilled water and dried in an oven at 373 K for 12 h.

All the synthesized zeolites were calcined at 853 K for 4 h in air and then ion-exchanged to the NH_4^+ form with 1 M NH_4NO_3 aqueous solution corresponding to the five-fold access of NH_4^+ for the Al content in zeolites. The exchange treatment was repeated three times. The NH_4^+-exchanged zeolites were calcined at 823 K in air for conversion to the proton form.

Commercial beta zeolites were calcined at 823 K in a stream of air.

All samples under study are denoted as X-ABC-n, where X = C (for conventional zeolites) or N (nanosponge), ABC is the zeolite framework types (**BEA***, **MTW** or **MFI**) and n = Si/Al ratio.

2.3. Characterization

X-ray powder diffraction (XRD) patterns were obtained with a Rigaku Multiflex diffractometer using Cu Kα radiation (λ = 0.1541 nm) at 30 kV and 40 mA (1.2 kW). Scanning electron micrograph (SEM) images were taken with a Verios 460 SEM microscope under operating condition at 1 kV (decelerating voltage: 3.0 kV) without a metal coating. High-resolution TEM (HR-TEM) images were taken with a FEI Tecnai G2 F30 microscope at an acceleration voltage of 300 kV. For TEM imaging, the powder samples were suspended in acetone by sonication and the solution was dropped on a holey carbon grid.

The nitrogen adsorption-desorption isotherms were obtained at 77 K with a Micromeritics Tristar II instrument. For adsorption measurements, the samples were degassed in vacuum at 573 K for 6 h. The specific surface area was calculated from the adsorption branch in the P/P_0 range between 0.01 and 0.30 using the Brunauer-Emmett-Teller (BET) equation. Approximate pore size distributions were derived from the adsorption branch according to the Barrett-Joyner-Halenda (BJH) algorithm. The argon sorption measurement was performed using a Micromeritics ASAP 2020 instrument at 87 K. For the Ar adsorption measurements, the samples were degassed in vacuum at

573 K for 6 h. The micropore volume and average micropore diameter of the catalysts were determined according to the nonlocal density functional theory (NLDFT).

The Si/Al ratio was determined by inductively coupled plasma-optical emission spectrometry (ICP-OES) using an iCAP 6300 Duo instrument (Thermo Scientific Co., UK). For the ICP analysis, the zeolite samples were completely dissolved in a dilute acid solution containing hydrochloric acid, nitric acid and hydrofluoric acid. To this clear solution, boric acid was added and dissolved completely to prevent the damage of ICP sample transport system by the complexation of the fluoride.

The concentration of Lewis and Brønsted acid sites was determined by Fourier transform infrared (FTIR) spectroscopy using a Nicolet Protégé 460 Magna equipped with a transmission MCT/A detector after adsorption of pyridine. For FTIR measurement, zeolite samples were pressed into self-supporting wafers with a density of 8.0 - 12 mg cm^{-2} and then activated in situ at 723 K and high vacuum (10^{-5} Torr) during 4 h. Pyridine adsorption was carried out at 423 K for 20 min at a partial pressure of 3.3 Torr. Then, the samples were degassed at 423 K for 20 min. The stepwise thermal desorption of the probe molecule was monitored by evacuating the sample at 423, 523, 623 and 723 K and cooling sample to room temperature between each step. Pyridine was purified through Freeze-pump-thaw cycles. All the spectra were recorded with a resolution of 4 cm^{-1} by collecting 128 scans for a single spectrum at room temperature. The spectra were normalized to a wafer density of 10 mg cm^{-2}. The concentration of Lewis and Brønsted acid sites was evaluated from the integral intensities of bands at 1454 cm^{-1} (Lewis acid sites) and at 1545 cm^{-1} (Brønsted acid sites) using extinction coefficients, $\varepsilon(L) = 2.22$ cm μmol^{-1} and $\varepsilon(B) = 1.67$ cm μmol^{-1} [43].

Thermogravimetric analysis (TGA) was carried out using a TGA Q50 (Thermal Analysis Instruments Inc.). The temperature was increased to 1073 K at a constant ramping rate of 20 K min^{-1} under air flow (60 ml min^{-1}).

2.4. Catalytic measurements

The tetrahydropyranylation reaction of alcohols with DHP was performed in the liquid phase at 300 or 333 K under atmospheric pressure in a multi-experiment workstation StarFish (Radleys Discovery Technologies). Before use, the catalyst was activated at 723 K for 90 min at a rate of 5 K min^{-1}. The alcohol, mesitylene (internal standard), hexane (solvent) and DHP were placed in a three-necked vessel equipped with a thermometer. After the solution reached the reaction temperature, the activated zeolite catalyst was added into the vessel. The details of reaction conditions for different kinds of alcohol are shown in the Table 1. Particular reaction conditions for each alcohol were established, where the reaction temperature or relative amount of the alcohol and DHP were systematically changed to show a comparative activity between hierarchical and commercial beta zeolites (Table 1). Samples of the reaction mixture were taken periodically and centrifuged. The liquid part was analyzed using an Agilent 6850 GC equipped with a nonpolar DB-5 column (length 20 m, diameter 0.180 mm and film thickness 0.18 mm) and a flame ionization detector. The GC analysis proceeded using 10 µl of injection volumes, 20 K min^{-1} of oven ramp rates from 333 K to 573 K and 4 min of hold times. The reaction products were identified by using a Thermo Finnigan Focus DSQ II single quadrupole GC/MS. The conversion and selectivity were calculated on the basis of the GC analysis. The conversion of alcohols was calculated

based on the amount of converted alcohol reactants using internal standard. The selectivity was determined using the response factors of the products. The deviation of the carbon balance calculated from the alcohol consumption and the sum of all products was smaller than ±5% in all experiments.

2.5. Recyclability test

The recyclability of the zeolite beta nanosponge with Si/Al = 110 was tested in the tetrahydropyranylation of 1-octanol with DHP at 333 K. After 1 h of reaction, the catalyst was separated from the reaction mixture by centrifugation and washed with hexane and acetone several times. The collected sample was dried at 423 K for 6 h. In the 2nd catalytic run, the sample was used without further activation at high temperature. Before the 3rd and 4th cycles, the used catalyst was calcined at 853 K for 4 h in air flow to remove the organic residues and subsequently activated at 723 K for 90 min.

3. Results and discussion

3.1. Structural and textural properties of the zeolites

Figs. 1A and 1B show representative SEM and TEM images of the nanosponge beta zeolite with Si/Al = 110 (N-**BEA***-110). The images display no visible additional phases. The SEM image of N-**BEA***-110 exhibits that the sample was composed of very thin nanocrystals of approximately 10 – 20 nm. The nanocrystals were randomly interconnected forming a nanosponge-like assembly. On the other hand, the SEM image of C-**BEA***-103 indicates that the sample consisted of aggregates (0.5 – 1 μm) of the particles with a diameter of 30 – 50 nm (Fig. 1C). The powder XRD patterns of N-**BEA***-110 and C-**BEA***-103 are shown in Fig. 1D. The wide-angle XRD pattern of C-**BEA***-103 sample exhibited several representative Bragg reflections, which are in a good agreement with those of the beta zeolites in the literature [44]. Compared to the C-**BEA***-103, the N-**BEA***-110 showed a broad small-angle peak at about 2θ = 1.4°, indicating that the nanosponge had modest mesostructural order. In addition, the wide-angle XRD pattern of the N-**BEA***-110 sample exhibited that characteristic Bragg diffraction lines (2θ = 7.5° and 22°) of the beta nanosponge sample were attributed to the small crystal domains of nanomorphic beta zeolite. However, other reflections corresponding to the beta zeolite structure could not be identified due to the broadening and low intensity of the peaks [35,40].

Textural properties of the N-**BEA***-110 and C-**BEA***-103 samples were evaluated using N_2 adsorption and desorption isotherm measured at 77 K (Fig. 1E). The isotherm exhibited a sharp increase in the adsorbed amount in the low pressure region of $P/P_0 <$ 0.1 and a gradual rise in the range of $0.4 < P/P_0 < 0.6$, followed by the hysteresis loop. The increase in the adsorbed amount in the low and high relative pressure region can be attributed to the filling of micropores and capillary condensation in the mesopores of the zeolite, respectively. The mesopore size distribution of nanosponge obtained by the BJH algorithm showed the peak centered at 4.5 nm. The N-**BEA***-110 sample possessed high BET area (770 m^2 g^{-1}) and external surface area (540 m^2 g^{-1}) determined using the *t*-plot method. The micropore volume (V_{mic}) and average micropore diameter (D_{mic}) were accurately assessed from Ar adsorption measurement at 87 K in the range of P/P_0

< 0.01. The values (V_{mic} = 0.18 cm^3 g^{-1}, D_{mic} = 0.64 nm) determined according to a NLDFT method corresponded to a typical microporous feature of beta zeolite (See Table 2 and Fig. S1) [33,45]. The results revealed that the nanosponge beta zeolite had highly hierarchical meso-microporous structure.

The nanosponge beta zeolites with different Si/Al ratios of 15 and 53 (N-**BEA***-15 and N-**BEA***-53, respectively) exhibited very similar morphologies in SEM and TEM images and reflections in the XRD patterns (Figs. S2 and S3). Both N-**BEA***-15 and N-**BEA***-53 samples also showed mesoporous characteristics similar to that of the N-**BEA***-110, possessing high BET areas (770 and 850 m^2 g^{-1}), external surface areas (580 and 590 m^2 g^{-1}) and large total pore volumes (1.3 and 1.4 cm^3 g^{-1}), respectively (Fig. S3 and Table 2).

In comparison with N-**BEA*** zeolites, the N_2 adsorption-desorption isotherm of C-**BEA***-103 exhibited type I isotherm (Fig. 1E), indicating a typical feature of microporous material although the sample did not show the smooth surface in the SEM image (Fig. 1C). C-**BEA***-103 also displayed considerably smaller external surface area (77 m^2 g^{-1}), compared with the nanosponge beta samples (Table 2). For the conventional beta zeolite with Si/Al = 20 (C-**BEA***-20), the morphology was similar with the C-**BEA***-103, representing the aggregation of zeolite crystals with a diameter ranging from 30 – 80 nm (Fig. S4). The C-**BEA***-20 possessed typically microporous structures and thereby had low external surface area (58 m^2 g^{-1}) and small pore volume (0.29 cm^3 g^{-1}) (Fig. S4 and Table 2).

Nanosponge zeolites with **MTW** and **MFI** structure were similarly characterized by SEM, TEM, XRD and N_2 adsorption analysis. The N-**MTW**-110 and N-**MFI**-80 materials exhibited a nanosponge-like morphology in which the zeolite nanocrystals were randomly assembled (Figs. S5A and S5D). The N-**MTW**-110 consisted of the nanocrystals with thicknesses of < 10 nm, which were assembled in a disordered manner. The N-**MFI**-80 was composed of the randomly self-connected zeolite nanolayers with 2.5 nm thickness exhibiting intercrystalline mesopores. The XRD patterns of the N-**MTW**-110 and N-**MFI**-80 samples exhibited the characteristic Bragg reflections corresponding to the **MTW** and **MFI** zeolite structures [37,38,41]. In addition, the both diffraction patterns showed the peak (2θ = 1.1° and 1.3°, respectively) in small-angle region of the XRD pattern, indicating that the nanosponge zeolites possessed a mesoporous structure (Figs. S5B and S5E) [36-38]. In a good agreement with the XRD and TEM analysis, N-**MTW**-110 and N-**MFI**-80 samples exhibited both inherent microporosity of the zeolites and mesoporous characteristics, corresponding to the hysteresis loops in the adsorption isotherms and narrow distributions of mesopore diameters centered at 4 nm (Table 2, Figs. S5C and S5F) [37,38]. Accordingly, the mesoporous **MTW** and **MFI** zeolites had high BET surface area and external surface area (Table 2).

3.2. Acidic properties of the zeolites

The concentration and type of acid sites in the conventional beta and nanosponge zeolites (beta, **MTW** and **MFI**) were determined by FTIR spectroscopy using pyridine

as a probe molecule. The pyridine with a kinetic diameter of about 0.5 nm can enter not only the 12-ring channels of the **BEA** (0.66 x 0.67 nm; 0.56 x 0.56 nm) and **MTW** (0.57 x 0.61 nm) zeolite but also 10-ring channels of the **MFI** (0.53 x 0.56 nm; 0.51 x 0.55 nm) zeolite [46,47]. Fig. 2 shows the concentrations of Lewis and Brønsted acid sites in the N-**BEA*** and C-**BEA*** samples, which were calculated from the integral intensities of the bands at 1454 and 1545 cm^{-1}, respectively, by using extinction coefficients reported in the literature [43]. For both nanosponge and conventional beta zeolites, with decrease of the Si/Al ratio of the zeolites, the total amounts of acid sites increased (N-**BEA***-15 > N-**BEA***-53 > N-**BEA***-110 and C-**BEA***-20 > C-**BEA***-103). This result showed a good agreement with the Al contents of the nanosponge and conventional beta samples, determined by ICP-OES (Table 2). Notably, all the nanosponge beta zeolites possessed significantly higher Lewis/Brønsted acid centers ratio in comparison to that in the conventional analogues. This feature can be attributed to the increased concentration of the defect sites in the hierarchical beta nanosponge zeolites [48]. The amounts of the Lewis and Brønsted acid centers in N-**MTW**-110 and N-**MFI**-80 samples were comparable with that in the N-**BEA***-110 possessing similar Si/Al ratio (Fig. S6).

The acid properties related to the relative strength of acid sites in the conventional and nanosponge zeolites were further investigated by thermal desorption of the adsorbed pyridine with the increase of desorption temperature from 423 K to 723 K. The IR spectra and acid concentrations calculated from the evaluation of the IR spectra in the range of 1400 cm^{-1} to 1600 cm^{-1} are shown in the Fig. S7 and Table S2. As shown in Table S2, the amount of acid sties was decreased systematically as the desorption temperature increased for both Lewis and Brønsted acid sites in the zeolites. For all the zeolites, the concentration of Lewis acid sites was relatively high in comparison with the Brønsted acid sites after pyridine desorption at 723 K. This can be explained by the general mechanism based on the increasing the number of Lewis acid sites with decrement of the bridged Si-OH-Al sites, associated with Brønsted acid sites [49]. Furthermore, all the zeolite samples possessed the reasonable amount of medium to strong acid sites, which was indicated by maintenance of the ratio of acid sites detected at 623 and 423 K (*i. e.*, C_{623}/C_{423}) in the range of 0.5 – 0.9 for both Lewis and Brønsted acid (Table S2). In the case of beta zeolites with different Si/Al ratios, the ratios of C_{623}/C_{423} tend to be increased with the increase of Si/Al ratio of the zeolite. Such tendency can be due to either lower stability of the zeolite framework or lower acid strength of the surface acid sites, regarding the close proximity of Al sites for the zeolite with low Si/Al ratios [50].

3.3. Catalytic performance of nanosponge beta zeolites in tetrahydropyranylation reaction

3.3.1. Comparison of catalytic performance between nanosponge and conventional beta zeolites

Catalytic properties of nanosponge and conventional beta zeolites were investigated in the liquid-phase tetrahydropyranylation of 1-octanol with DHP. Both Lewis and Brønsted acid sites can act as active centers in this reaction (Scheme 2) [17,51]. Fig. 3A

shows the catalytic results obtained over N-**BEA***-110 and C-**BEA***-103 by means of conversion of 1-octanol plotted as a function of reaction time. The plot displays that the 1-octanol conversion over N-**BEA***-110 and C-**BEA***-103 catalysts increased in the 30 min of the initial reaction period. After initial reaction period, the catalytic conversion increased gradually with the reaction time and converged to a maximum value. The N-**BEA***-110 exhibited a significantly higher catalytic conversion than the C-**BEA***-103 (56% vs. 16%, respectively) at 24 h of reaction time. This result is consistent with previous report showing that the nanosponge beta zeolite exhibits higher catalytic conversion in Friedel-Crafts alkylation reaction of aromatics than conventional beta zeolite catalyst [41]. The N-**BEA***-110 and C-**BEA***-103 showed a comparable selectivity (90 – 100%) to the desired tetrahydropyranyl ether during the whole reaction time. C-**BEA***-103 was deactivated rapidly, indicating the maximum value of the conversion of reactant within 30 min. The result well corresponded to the data obtained from TGA analysis where the spent catalyst possessed substantial amounts of carbonaceous materials within 30 min of the reaction time (Fig. S8). Thus, the rapid deactivation of C-**BEA***-103 can be explained by limitation of the accessibility of reactants to the active sites by formation of polymeric compounds as cokes in the micropores. This was the main reason of the rapid deactivation for microporous zeolites in various catalytic reactions [52-54]. We calculated 'total number of reactant alcohol molecules converted per acid site' during 24 h (*i. e.* turnover number, 'TON') and 'the number of reactant molecules per total acid sites per unit time (h) (*i. e.* turnover frequency, 'TOF') based on the total concentration of both Lewis and Brønsted acid sites accessible for pyridine molecules (Fig. 2). The reaction for determination of the TOF was carried out in a mild condition by reducing the amount of catalyst and reaction temperature owing to significantly high reactivity (above 30% conversion within 15 min) in the reaction condition described in Table 1. The TOF was calculated using the linear part of the conversion-time dependence (in the range of < 10% conversion) to exclude the influence of deactivation (inset in Fig. 3A). Fig. 3B shows the TON and TOF of N-**BEA***-110 and C-**BEA***-103 in the tetrahydropyranylation reaction of 1-octanol. The result was obtained taking into consideration that a deviation within 5% was calculated from a set of three different experiments. As the conversion of N-**BEA***-110 constantly increased in contrast to C-**BEA***-103 (Fig. 3A), the TON value of N-**BEA***-110 (584) was much higher than that of C-**BEA***-103 (171). This result may be related to the well-developed mesopore structure and large external surface of the hierarchical zeolite facilitating easier diffusion of reactants and products, and therefore a slow rate of deactivation. In addition, the N-**BEA***-110 showed about 2-fold higher TOF (111 $x10^{-2}$, h^{-1}) in comparison with C-**BEA***-103 (64 $x10^{-2}$, h^{-1}). The higher catalytic activity of N-**BEA***-110 can be attributed to the high concentration and accessibility of the active sites located on the external surface of nanosponge zeolite.

In order to investigate the influence of the reactant molecule size on the catalytic behavior of bulk and nanomorphic materials, different alcohols (methanol, cyclohexanol and 2-adamantanol) have been used in the tetrahydropyranylation reaction (Table 1). The TOF and TON values of N-**BEA***-110 and C-**BEA***-103 were evaluated for each reaction (Table 3). For both conventional and nanosponge samples, catalytic activity gradually decreased with increase of alcohol size ($TOF_{methanol} > TOF_{cyclohexanol} \approx TOF_{1\text{-}octanol} > TOF_{2\text{-}adamantanol}$). Similarly to the results obtained in the tetrahydropyranylation

of 1-octanol, N-**BEA***-110 exhibited higher values of the TOF and TON compared to C-**BEA***-103 for all the alcohols applied. This difference became especially pronounced when the most bulky 2-adamantanol was used: $TOF_{N\text{-}\mathbf{BEA}^*\text{-}110}/TOF_{C\text{-}\mathbf{BEA}^*\text{-}103}$ increased to 4.1 from 2.3 – 2.7 characteristic for transformation of methanol and cyclohexanol. These results confirmed the preferences of nanosponge materials over conventional zeolites in terms of diffusional limitations and accessibility of acid sites mentioned above.

3.3.2. Effect of Si/Al ratio in nanosponge beta zeolites

The catalytic behavior of nanosponge beta zeolites with different Si/Al ratio (N-**BEA***-15, N-**BEA***-53 and N-**BEA***-110) was investigated in the tetrahydropyranylation of different alcohols (methanol, 1-octanol, cyclohexanol and 2-adamantanol). In all reactions, with increasing the Al content in the N-**BEA*** samples, the yield of tetrahydropyranyl ether increased, which was reasonable in accordance with increase in the total acid site concentrations (Figs. 2 and S9). For all of used alcohols, both TOF and TON values increased with decreasing Al contents (N-**BEA***-15 < N-**BEA***-53 < N-**BEA***-110) (Fig. 4). This tendency of decreased catalytic activities with increasing Al content is commonly known in acid-catalyzed reaction over zeolites, which can be due to the closely located Al sites and/or reduced hydrophobicity in zeolite frameworks [55,56]. Similarly, Kim *et al*. reported such tendencies of the catalytic activity in the Pechmann condensation reaction over the nanosponge **MFI** zeolites with different Si/Al ratios [57].

3.3.3. Effect of the framework type of nanosponge zeolite

We performed the tetrahydropyranylation reaction of 1-octanol and 2-adamantanol over the beta, **MTW** and **MFI** nanosponge zeolites in order to investigate the effect of framework topology of the zeolite. In the case of 1-octanol, N-**BEA***-110 and N-**MTW**-110 exhibited higher yields of tetrahydropyranyl ether in comparison with N-**MFI**-80 during whole reaction time (Fig. S10A). The TOF and TON values of N-**BEA***-110 (TOF = 111 $x10^{-2}$, h^{-1}, TON = 584) and N-**MTW**-110 (TOF = 89 $x10^{-2}$, h^{-1}, TON = 613) were also higher than those of N-**MFI**-80 (TOF = 40 $x10^{-2}$, h^{-1}, TON = 428) (Fig. 5A). On the other hand, the catalytic performance of the nanosponge zeolites showed a notable difference in the tetrahydropyranylation of 2-adamantanol (Fig. S10B). N-**BEA***-110 (TOF = 74 $x10^{-2}$, h^{-1}, TON = 529) exhibited the highest catalytic activity, presenting the higher TOF and TON values than N-**MTW**-110 (TOF = 27 $x10^{-2}$, h^{-1}, TON = 370) and N-**MFI**-80 (TOF = 7.6 $x10^{-2}$, h^{-1}, TON = 224) (Fig. 5B). The results indicate that the nanosponge **MTW** and especially beta zeolites showed a better catalytic performance rather than the nanosponge **MFI** zeolite possessing the larger amount of total acid sites (Figs 3 and S6). This observation can be ascribed to the differences in the pore structure of zeolites used. While the beta zeolite possessed 3-dimensionally (3D) intersecting pore structure composed of 12-ring channels, pore structure of the **MTW** (1D, 12-ring) and **MFI** (3D, 10-ring) zeolites resulted in the

diffusional obstructions for reactant and product molecules. As a result, the catalytic activities of the nanosponge beta, **MTW** and **MFI** zeolites can be said to be dependent on their intrinsic pore structures, considering that the three nanosponge zeolites possessed enough high external surface area and large mesopores for the tetrahydropyranylation reaction of linear alkyl and bulky cyclic alcohols.

3.4. Recycling test

The recyclability of N-**BEA***-110 was studied in the tetrahydropyranylation reaction of 1-octanol with DHP. After the first kinetic run, the used sample was washed with organic solvent (hexane and acetone) and then dried only at 423 K without further activation at high temperature. The catalytic conversion in 2nd cycle decreased to 15.2 % from that obtained in the 1st cycle (41.7 %), while the selectivity was maintained during the recycling runs. The deactivation can be attributed to pore blocking by organic compounds since the catalyst collected after the first reaction showed weight loss of 20 % by thermal decomposition as confirmed by TGA analysis (Fig. S11). The collected sample therefore was calcined at 853 K under air atmosphere to remove the organic compounds before 3rd cycling test. The catalytic activity of the calcined catalyst could be recovered to 96 % of original activity in the 3rd cycle. In addition, the recyclability was preserved until the 4th cycle, exhibiting a negligible difference in conversion of 1-octanol from the 3rd cycle. In accordance with the recyclability of N-**BEA***-100, the catalyst collected after 3rd or 4th cycle and subsequent calcination exhibited the maintenance of the mesostructure and crystallinity as well as acid properties, comparable to the fresh catalyst (Figs. S12 and S13). Therefore, the nanosponge beta zeolite could be regenerated by the calcination, showing the recovered catalytic activity in recycle test (Table 4).

4. Conclusions

The nanosponge beta zeolites with a meso-micro hierarchical structure were synthesized using piperidinium-functionalized multi-ammonium surfactants as SDAs. The resulting beta nanosponges possessed large surface areas and uniform mesopores. In the liquid-phase tetrahydropyranylation of alcohols (methanol, 1-octanol, cyclohexanol and 2-adamantanol) with 3,4-dihydro-2H-pyran, the beta nanosponges exhibited enhanced catalytic performance with the higher conversion and initial reaction rate compared to the conventional beta catalyst.

Remarkable enhancement of the catalytic activity of the nanosponge was found in the tetrahydropyranylation reaction of bulky alcohol (*e.g.* 2-adamanthanol), which can be attributed to high accessibility of the active sites and facile diffusion of reactant and product molecules in the mesoporous beta zeolites. Furthermore, the catalytic behavior of nanosponge beta zeolites with different Si/Al ratios showed a measurable relationship with increase in the Al contents, evidencing the decrease of TOF and TON or increase in the yield toward target ethers. Notably, the beta nanosponge exhibited superior catalytic activity in the tetrahydropyranylation reaction of 1-octanol and 2-adamantanol in

comparison with mesoporous **MTW** and **MFI** zeolites, exhibiting higher initial reaction rate. We postulate that the enhanced catalytic activity of beta nanosponge can be the result of the intrinsic pore structure of the nanosponge beta zeolite (3D, 12-ring) different from nanosponge **MTW** (1D, 12-ring) and **MFI** (3D, 10-ring) zeolites, considering their high external surface areas, large mesopores and comparable acidic properties.

Acknowledgements

JČ thanks the Czech Science Foundation for the support of this research (P106/12/0189). R.R. acknowledges the Institute for Basic Science (IBS-R004-D1).

References

[1] B. Kumar, M.A. Aga, A. Rouf, B.A. Shah, S.C. Taneja, *RSC Adv.* 4 (2014) 21121-21130.
[2] R. Schwalm, H. Binder, D. Funhoff, *J. Appl. Polym. Sci.* 78 (2000) 208-216.
[3] A.T. Khan, T. Parvin, L.H. Choudhury, *Synthesis* 15 (2006) 2497-2502.
[4] H.S. Mason, *J. Am. Chem. Soc.* 69 (1947) 2241-2242.
[5] R. Sanz, A. Martínez, J.M. Álvarez-Gutiérrez, F. Rodríguez, *Eur. J. Org. Chem.* 2006 (2006) 1383-1386.
[6] A.K. Banerjee, W. Vera, H. Mora, M.S. Laya, L. Bedoya, E.V. Cabrera, *J. Sci. Ind. Res.* 65 (2006) 299-308.
[7] K. Nagaiah, B. V. S. Reddy, D. Sreenu, A. Venkat Narsaiah, *ARKIVOC* 2005 (2005) 192-199.
[8] S. Chandrasekhar, Mohamed Takhi, Y. Ravindra Reddy, Suchismita Mohapatra, C. Rama Rao, K. Venkatram Reddy, *Tetrahedron* 53 (1997) 14997-15004.
[9] T.W. Green, P.G.M. Wuts, *Protective groups in organic synthesis*, 3rd edn. John Wiley, New York (1999) 42-62.
[10] N. Narender, K. Suresh Kumar Reddy, M. Arun Kumar, C. N. Rohitha, S. Kulkarni, *Catal. Lett.* 134 (2010) 175-178.
[11] K. Shimizu, E. Hayashi, T. Hatamachi, T. Kodama, Y. Kitayama, *Tetrahedron Lett.* 45 (2004) 5135-5138.
[12] A. Cornelis, P. Laszlo, *Synlett* (1994) 155-161.
[13] S. Hoyer, P. Laszlo, M. Orlović, E. Polla, *Synthesis* (1986) 655-657.
[14] R. Ballini, F. Bigi, S. Carloni, R. Maggi, G. Sartori, *Tetrahedron Lett.* 38 (1997) 4169-4172.
[15] P. Kumar, C.U. Dinesh, R.S. Reddy, B. Pandey, *Synthesis* (1993) 1069-1070.
[16] P. Kumar, S.V.N. Raju, R.S. Reddy, B. Pandey, *Tetrahedron Lett.* 35 (1994) 1289-1290.
[17] G. Sartori, R. Ballini, F. Bigi, G. Bosica, R. Maggi, P. Righi, *Chem. Rev.* 104 (2004) 199-250.
[18] J.-E. Choi, K.-Y. Ko, *Bull. Korean Chem. Soc.* 22 (2001) 1177-1178.

[19] J.M. Campelo, A. Garcia, F. Lafont, D. Luna, J.M. Marinas, *Synth. Commun.* 22 (1992) 2335-2342.
[20] D. Nedumaran, A. Pandurangan, *Micropor. Mesopor. Mater.* 169 (2013) 25-34.
[21] I. Rodriguez, M.J. Climent, S. Iborra, V. Fornés, A. Corma, *J. Catal.* 192 (2000) 441-447.
[22] M.V. Shamzhy, M.V. Opanasenko, F.S.de O. Ramos, L. Brabec, M. Horacek, M. Navarro-Rojas, R.E. Morris, H.de O. Pastore, J. Cejka, *Catal. Sci. Technol.* 5 (2015) 2973-2984.
[23] J. Pérez-Ramírez, C.H. Christensen, K. Egeblad, C.H. Christensen, J. C. Groen, *Chem. Soc. Rev.* 37 (2008) 2530-2542.
[24] A. Corma, *J. Catal.* 216 (2003) 298-312.
[25] P. Eliasova, M. Opanasenko, P.S. Wheatley, M. Shamzhy, M. Mazur, P. Nachtigall, W.J. Roth, R.E. Morris, J. Cejka *Chem. Soc. Rev.* 44 (2015) 7177-7206.
[26] Y. Tao, H. Kanoh, L. Abrams, K. Kaneko, *Chem. Rev.* 106 (2006) 896-910.
[27] Y. Wei, P.E. de Jongh, M.L.M. Bonati, D.J. Law, G.J. Sunley, K.P. de Jong, *Appl. Catal., A* 504 (2015) 211-219.
[28] S. van Donk, A.H. Janssen, J.H. Bitter, K.P. de Jong, *Catal. Rev.* 45 (2003) 297-319.
[29) C.J.H. Jacobsen, C. Madsen, J. Houzvicka, I. Schmidt, A. Carlsson, *J. Am. Chem. Soc.* 122 (2000) 7116-7117.
[30] H. Wang, T.J. Pinnavaia, *Angew. Chem. Int. Ed.* 45 (2006) 7603-7606.
[31] M. Choi, H.S. Cho, R. Srivastava, C. Venkatesan, D.-H. Choi, R. Ryoo, *Nature Mater.* 5 (2006) 718-723.
[32] K. Cho, H.S. Cho, L.-C. de Menorval, R. Ryoo, *Chem. Mater.* 21 (2009) 5664-5673.
[33] D. P. Serrano, J. M. Escola, P. Pizarro *Chem. Soc. Rev.* 42 (2013) 4004-4035.
[34] M. Choi, K. Na, J. Kim, Y. Sakamoto, O. Terasaki, R. Ryoo, *Nature* 461 (2009) 246-249.
[35] K. Na, C. Jo, J. Kim, K. Cho, J. Jung, Y. Seo, R.J. Messinger, B.F. Chmelka, R. Ryoo, *Science* 333 (2011) 328-332.
[36] C. Jo, Y. Seo, K. Cho, J. Kim, H.S. Shin, M. Lee, J.-C. Kim, S.O. Kim, J.Y. Lee, H. Ihee, R. Ryoo, *Angew. Chem., Int. Ed.* 53 (2014) 5117-5121.
[37] C. Jo, K. Cho, J. Kim, R. Ryoo, *Chem. Commun.* 50 (2014) 4175-4177.
[38] W. Kim, J.-C. Kim, J. Kim, Y. Seo, R. Ryoo, *ACS Catal.* 3 (2013) 192-195.
[39] M.V. Opanasenko, M.V. hamzhy, C. Jo, R. Ryoo, J. Cejka, *ChemCatChem.* 6 (2014) 1919-1927.
[40] C. Jo, W. Park, R. Ryoo, *Micropor. Mesopor. Mater.* 239 (2017) 19-27.
[41] J.-C. Kim, K. Cho, R. Ryoo, *Appl. Catal., A* 470 (2014) 420-426.
[42] T.-W. Kim, S.-Y. Kim, J.-C. Kim, Y. Kim, R. Ryoo, C.-U. Kim, *Appl. Catal., B* 185 (2016) 100-109.
[43] C.A. Emeis, *J. Catal.* 141 (1993) 347-354.
[44] B. Yilmaz, U. Muller, M. Feyen, S. Maurer, H. Zhang, X. Meng, F.-S. Xiao, X. Bao, W. Zhang, H. Imai, T. Yokoi, T. Tatsumi, H. Gies, T.D. Baerdemaeker, D.D. Vos, *Catal. Sci. Technol.* 3 (2013) 2580-2586.
[45] K. Gora-Marek, K. Tarach, M. Choi, *J. Phys. Chem. C* 118 (2014) 12266-12274.
[46] J.C. Jansen, E.J. Creyghton, S.L. Njo, H. Koningsveld, H. Bekkum, *Catal. Today* 38 (1997) 205-212.
[47] B.H. Chiche, R. Dutartre, F.D. Renzo, F. Fajula, *Catal. Lett.* 31 (1995) 359-366.

[48] R.A. Garcia-Munoz, D.P. Serrano, G. Vicente, M. Linares, D. Vitvarova, J. Cejka, *Catal. Today* 243 (2015) 141-152.
[49] L. F. Isernia, *Mat. Res.* 16 (2013) 792-802.
[50] J. Dědeček , Z. Sobalík, B. Wichterlová, *Cat. Rev. - Sci. Eng.* 54 (2012) 135-223.
[51] P.G.M. Wuts, T.W. Greene, *Greene's Protective Groups in Organic Synthesis*, John Wiley $ Sons, Inc. (2006) 431-532.
[52] F.L. Bleken, K. Barbera, F. Bonino, U. Olsbye, K.P. Lillerud, S. Bordiga, P. Beato, T.V.W. Janssens, S. Svelle, *J. Catal.* 307 (2013) 62-73.
[53] M.D. Argyle, C.H. Bartholomew, *Catalysts* 5 (2015) 145-269.
[54] M. Xu, C. Mukarakate, D.J. Robichaud, M.R. Nimlos, R.M. Richards, B.G. Trewyn, *Top. Catal.* 59 (2016) 73-85.
[55] M.V. Opanasenko, W.J. Roth, J. Čejka, *Catal. Sci. Technol.* 6 (2016) 2467-2484.
[56] W.J. Roth, P. Nachtigall, R.E. Morris, J. Čejka *Chem. Rev.* 114 (2014) 4807-4837.
[57] J.-C. Kim, R. Ryoo, M.V. Opanasenko, M.V. Shamzhy, J. Cejka, *ACS Catal.* 5 (2015) 2596-2604.

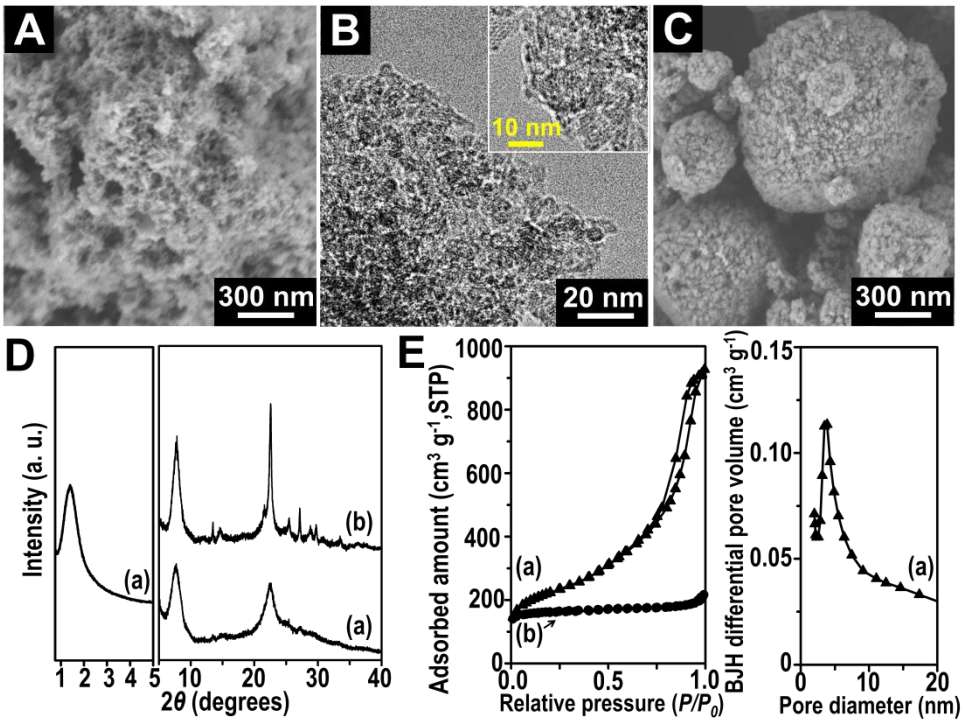

Fig. 1. SEM (A) and HR-TEM (B) images of N-**BEA***-110, SEM image (C) of C-**BEA***-103, small and wide angle XRD patterns (D) of N-**BEA***-110 (a) and C-**BEA***-103 (b), N_2 adsorption-desorption isotherm (E) of N-**BEA***-110 (a) and C-**BEA***-103 (b) and pore size distributions corresponding to the adsorption branch of N-**BEA***-110 (a).

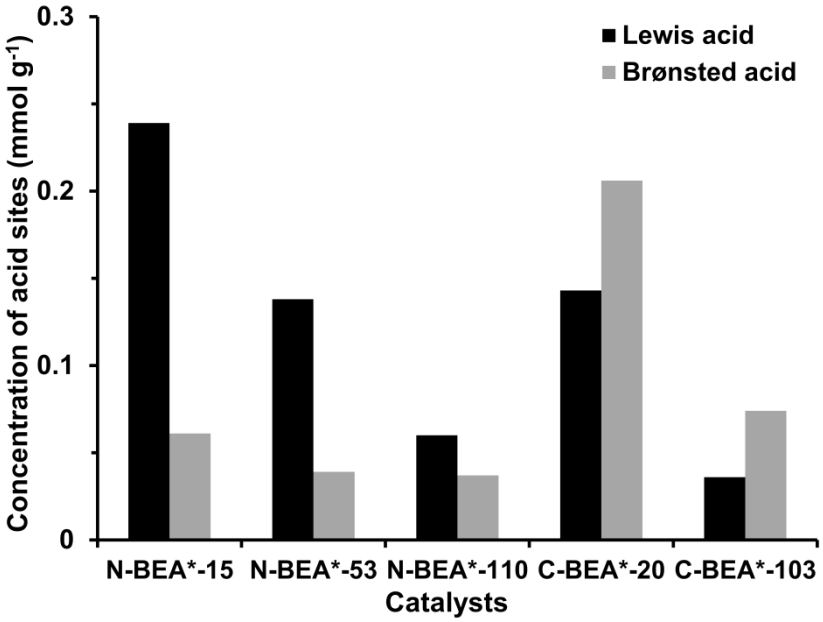

Fig. 2. Concentration of Brønsted and Lewis acid sites in nanosponge and commercial beta zeolites determined by FTIR spectroscopy using pyridine as a probe molecule.

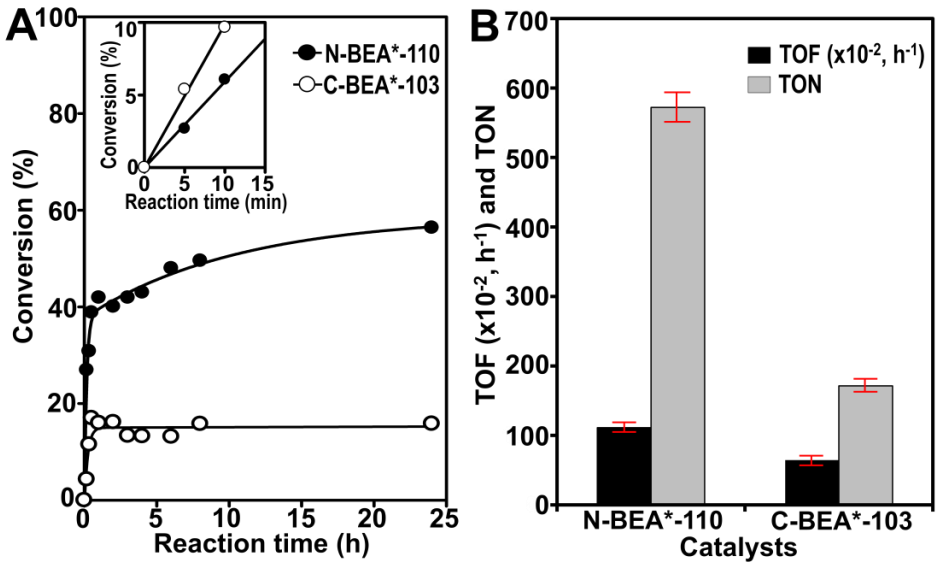

Fig. 3. Conversion of 1-octanol *versus* reaction time** (A) and TOF* and TON** (B) obtained in the tetrahydropyranylation reaction of 1-octanol with DHP over N-**BEA***-110 and C-**BEA***-103, respectively. The inset of (A) is conversion of 1-octanol over N-**BEA***-110 as a function of reaction time for determination of initial reaction rate *(i. e.*, TOF*). Error bars (red lines) in (B) represent the deviation within 5% calculated from a set of three different measurements. Reaction conditions: *5 mmol of 1-octanol, 15 mmol of DHP, 0.5 g of mesitylene (internal standard), 3 ml of hexane (solvent), 10 mg of catalyst, 300 K. **5 mmol of 1-octanol, 78 mmol of DHP, 0.5 g of mesitylene (internal standard), 50 mg of catalyst, 333 K.

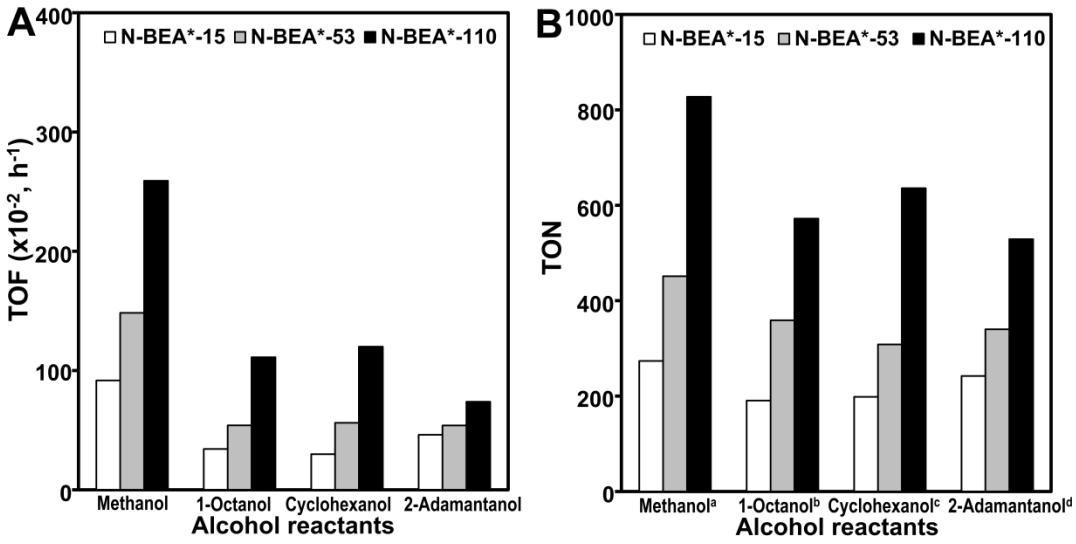

Fig. 4. TOF* (A) and TON** (B) obtained in the tetrahydropyranylation reaction of methanol, 1-octanol, cyclohexanol and 2-adamantanol with DHP over N-**BEA***-15, N-**BEA***-53 and N-**BEA***-110, respectively. Reaction conditions: *5 mmol of alcohol, 15 mmol of DHP, 0.5 g of mesitylene (internal standard), 3 ml of hexane (solvent), 10 mg of catalyst, 300 K. **9 mmol of [a]methanol, 15 mmol of DHP, 0.05 g of mesitylene (internal standard), 10 ml of hexane (solvent), 25 mg of catalyst, 300 K, 24 h. 5 mmol of [b]1-octanol, [c]cyclohexanol and [d]2-adamantanol, [b]78, [c]150 and [d]220 mmol of DHP, 0.5 g of mesitylene (internal standard), 50 mg of catalyst, 333 K, 24 h.

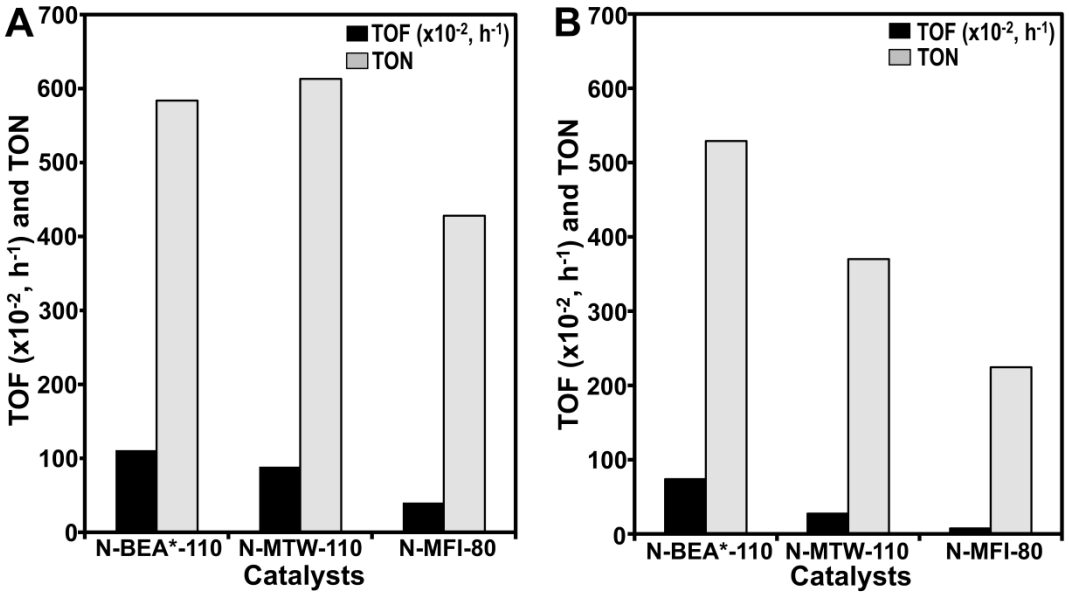

Fig. 5. TOF* and TON** obtained in the tetrahydropyranylation reaction of 1-octanol (A) and 2-adamantanol (B) with DHP over N-**BEA***-110, N-**MTW**-110 and N-**MFI**-80, respectively. Reaction conditions: *5 mmol of alcohol, 15 mmol of DHP, 0.5 g of mesitylene (internal standard), 3 ml of hexane (solvent), 10 mg of catalyst, 300 K. **5 mmol of [a]1-octanol and [b]2-adamantanol, [a]78 and [b]220 mmol of DHP, 0.5 g of mesitylene (internal standard), 50 mg of catalyst, 333 K, 24 h.

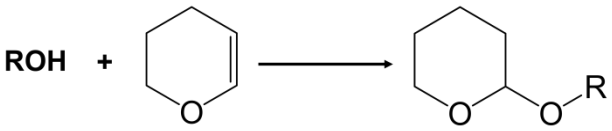

Scheme 1. Tetrahydropyranylation of alcohols with DHP over acid catalysts.

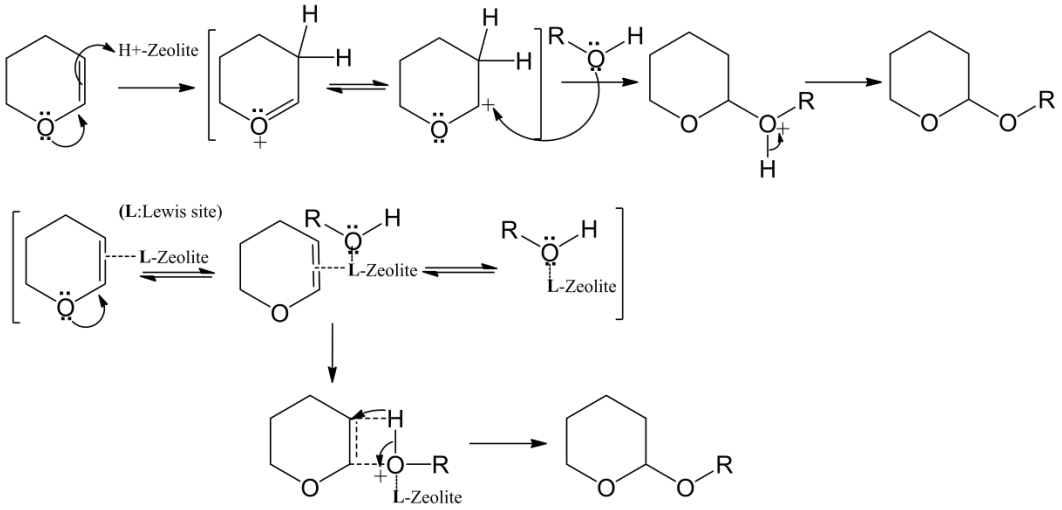

Scheme 2. Possible reaction mechanism of the tetrahydropyranylation of alcohols over zeolite catalysts.

Table 1. The reaction conditions for tetrahydropyranylation of the different kinds of alcohol.

Alcohol (mmol)	Mesitylene (g)	Hexane (ml)	DHP (mmol)	Catalyst (mg)	T (K)[a]
methanol (9)	0.05	10	15	25	300
1-octanol (5)	0.5	not used	78	50	333
cyclohexanol (5)	0.5	not used	150	50	333
2-adamantanol (5)	0.5	not used	220	50	333

[a] Reaction temperature.

Table 2. Physicochemical properties of nanosponge zeolites (**BEA***, **MTW** and **MFI**) and conventional beta zeolite catalysts.

Catalyst	Si/Al[a]	S_{BET} [b] ($m^2\ g^{-1}$)	S_{ext} [c] ($m^2\ g^{-1}$)	V_{tot} [d] ($cm^3\ g^{-1}$)	V_{mic} [e] ($cm^3\ g^{-1}$)
C-**BEA***-20	20	580	58	0.29	0.28
C-**BEA***-103	103	550	77	0.29	0.25
N-**BEA***-15	15	770	580	1.30	0.14
N-**BEA***-53	53	850	590	1.40	0.18
N-**BEA***-110	110	790	540	1.30	0.18
N-**MTW**-110	110	430	290	0.42	0.12
N-**MFI**-80	80	610	540	0.69	0.13

[a]The Si/Al molar ratio was determined by ICP-OES analysis. [b]S_{BET} is the BET surface area obtained from N_2 adsorption in the relative pressure range (P/P_0) of 0.1-0.3. [c]S_{ext} is the external surface area evaluated from the *t*-plot method. [d]V_{tot} is total pore volume obtained at $P/P_0 = 0.95$. [e]V_{mic} is the micropore volume, obtained from Ar adsorption at $P/P_0 < 0.01$. The V_{mic} was determined according to the NLDFT.

Table 3. TOF and TON obtained in the tetrahydropyranylation reaction of methanol, cyclohexanol and 2-adamantanol with DHP over N-**BEA***-110 and C-**BEA***-103, respectively.

Alcohol	Catalyst	TOF ($x10^{-2}$, h^{-1})[a]	TON
Methanol	N-**BEA***-110	259	827[b]
	C-**BEA***-103	97	319[b]
Cyclohexanol	N-**BEA***-110	120	571[c]
	C-**BEA***-103	53	375[c]
2-Adamantanol	N-**BEA***-110	74	529[d]
	C-**BEA***-103	18	198[d]

Reaction conditions: [a]5 mmol of alcohol, 15 mmol of DHP, 0.5 g of mesitylene (internal standard), 3 ml of hexane (solvent), 10 mg of catalyst, 300 K. [b]9 mmol of methanol, 15 mmol of DHP, 0.05 g of mesitylene (internal standard), 10 ml of hexane (solvent), 25 mg of catalyst, 300 K, 24 h. 5 mmol of [c]cyclohexanol and [d]2-adamantanol, [c]150 and [d]220 mmol of DHP, 0.5 g of mesitylene (internal standard), 50 mg of catalyst, 333 K, 24 h.

Table 4. Recyclability test of N-**BEA***-110 in the tetrahydropyranylation reaction* of 1-octanol with DHP.

Cycle	Conversion (%)
1	41.7
2[a]	15.2
3[b]	39.9
4[b]	38.7

*Reaction conditions: 5 mmol of 1-octanol, 78 mmol of DHP, 0.5 g of mesitylene (internal standard), 50 mg of catalyst, 333 K, 1 h. [a]For the 2nd cycle, the used catalyst was washed with hexane and acetone and then dried at 423 K for 6 h. [b]The 3rd and 4th cycles were carried out with the catalyst calcined at 853 K for 4 h in air flow after using in the previous reaction.